

Attribution-ShareAlike 4.0 International (CC BY-SA 4.0)

<https://creativecommons.org/licenses/by-sa/4.0/>

Access to this work was provided by the University of Maryland, Baltimore County (UMBC) ScholarWorks@UMBC digital repository on the Maryland Shared Open Access (MD-SOAR) platform.

Please provide feedback

Please support the ScholarWorks@UMBC repository by emailing scholarworks-group@umbc.edu and telling us what having access to this work means to you and why it's important to you. Thank you.



Regional Characteristics of NO₂ Column Densities from Pandora Observations during the MAPS-Seoul Campaign

Heesung Chong¹, Hana Lee¹, Ja-Ho Koo¹, Jhoon Kim^{1,2}, Ukkyo Jeong^{3,4}, Woogyung Kim^{3,4}, Sang-Woo Kim⁵, Jay R. Herman³, Nader K. Abuhassan³, Joon-Young Ahn⁶, Jeong-Hoo Park⁶, Sang-Kyun Kim⁶, Kyung-Jung Moon⁶, Won-Jun Choi⁶, Sang Seo Park^{5*}

¹ Department of Atmospheric Sciences, Yonsei University, Seoul 03722, Korea

² Harvard – Smithsonian Center for Astrophysics, Cambridge, MA 02138, USA

³ NASA Goddard Space Flight Center, Greenbelt, MD 20771, USA

⁴ Earth System Science Interdisciplinary Center, The University of Maryland, College Park, MD 20742, USA

⁵ School of Earth and Environmental Sciences, Seoul National University, Seoul 08826, Korea

⁶ National Institute of Environmental Research, Incheon 22689, Korea

ABSTRACT

Vertical column density (VCD) of nitrogen dioxide (NO₂) was measured using Pandora spectrometers at six sites on the Korean Peninsula during the Megacity Air Pollution Studies-Seoul (MAPS-Seoul) campaign from May to June 2015. To estimate the tropospheric NO₂ VCD, the stratospheric NO₂ VCD from the Ozone Monitoring Instrument (OMI) was subtracted from the total NO₂ VCD from Pandora. European Centre for Medium-Range Weather Forecasts (ECMWF) reanalysis wind data was used to analyze variations in tropospheric NO₂ VCD caused by wind patterns at each site. The Yonsei/SEO site was found to have the largest tropospheric NO₂ VCD (1.49 DU on average) from a statistical analysis of hourly tropospheric NO₂ VCD measurements. At rural sites, remarkably low NO₂ VCDs were observed. However, a wind field analysis showed that trans-boundary transport and emissions from domestic sources lead to an increase in tropospheric NO₂ VCD at NIER/BYI and KMA/AMY, respectively. At urban sites, high NO₂ VCD values were observed under conditions of low wind speed, which were influenced by local urban emissions. Tropospheric NO₂ VCD at HUFS/Yongin increases under conditions of significant transport from urban area of Seoul according to a correlation analysis that considers the transport time lag. Significant diurnal variations were found at urban sites during the MAPS-Seoul campaign, but not at rural sites, indicating that it is associated with diurnal patterns of NO₂ emissions from dense traffic.

Keywords: Pandora; NO₂; MAPS-Seoul.

INTRODUCTION

Nitrogen dioxide (NO₂) is an important chemical species in both tropospheric and stratospheric chemistry (e.g., Crutzen, 1979; Brasseur *et al.*, 1998). NO₂ mainly affects air quality in the troposphere through its role in chemical processes with ozone (O₃) and other trace gases (e.g., Seinfeld, 1988; Solomon *et al.*, 1999; IPCC, 2007; Choi *et al.*, 2008, 2009). In addition, long-term exposure to high concentrations of NO₂ causes respiratory and cardiovascular diseases (e.g., Chitano *et al.*, 1995; Bayram *et al.*, 2001; von Klot *et al.*, 2005). Emission sources of NO₂ differ between the troposphere and stratosphere (Lee *et al.*, 1997;

Barton and Atwater, 2002; Galloway *et al.*, 2004). In the stratosphere, the main source of NO₂ is oxidation of nitrous oxide (N₂O) and other sources include lightning and biomass burning (e.g., Liley *et al.*, 2000; Barthe *et al.*, 2007; Allen *et al.*, 2010; Bucsele *et al.*, 2013). In the troposphere, anthropogenic activities, including fossil fuel combustion and vehicle emissions, are the dominant sources of NO₂, along with some contributions from soil emissions and lightning (Zhang *et al.*, 2003; Hudman *et al.*, 2007; Choi *et al.*, 2008, 2009). Because of the diversity of nitrogen oxides chemical reactions and emission sources, spatial distributions of NO₂ typically show regional differences. For these reasons, accurate observations of the spatial distribution of NO₂ are important.

Several measurement platforms for tropospheric gases, including NO₂, have been developed in recent decades. In particular, tropospheric column NO₂ is widely monitored using ground- and satellite-based platforms that make use of the spectral absorption features of NO₂. For example,

*Corresponding author.

Tel.: 82-2-880-5743; Fax: 82-2-887-0210

E-mail address: pss8902@gmail.com

the Brewer spectrophotometer can estimate total column NO₂ using direct solar radiation at several specific wavelengths (e.g., Brewer *et al.*, 1973; Kerr *et al.*, 1988; Kerr, 1989; Cede *et al.*, 2006; Diemmoz *et al.*, 2014). In addition, several instruments have been used to measure NO₂ column densities using differential optical absorption spectroscopy (DOAS) methods (e.g., Boersma *et al.*, 2004; Castellanos *et al.*, 2015; Chimot *et al.*, 2016) applied to sunlight scattered along the zenith (Van Roozendaal *et al.*, 1997; Liley *et al.*, 2000) or scattered in multiple directions (e.g., Sinreich *et al.*, 2005; Irie *et al.*, 2008; Lee *et al.*, 2009a, b).

Recently, the Pandora spectrometer was developed by Goddard Space Flight Center (GSFC) at the National Aeronautics and Space Administration (NASA) for the estimation of trace gases using direct sunlight (Herman *et al.*, 2009; Cede, 2011). The Pandora system is an array detector spectrometer with a temperature control system. A solar tracking system is also included to allow constant direct-sunlight observations. Using this optical system, the Pandora instrument can continuously observe direct radiance with high temporal resolution. This instrument has been used to obtain the total column amount of trace gases, including O₃ and NO₂ (Herman *et al.*, 2009; Tzortziou *et al.*, 2012).

In South Korea, the first two Pandora instruments were installed in 2012 at Yonsei University in Seoul and Pusan National University in Busan for trace gas observations during the Distributed Regional Aerosol Gridded Observation Networks-North East Asia (DRAGON NE-Asia) campaign. Since the initial installations, several instruments were installed additionally in different regions in Korea. The main purpose of Pandora network in Korea was to conduct observations for the Megacity Air Pollution Studies-Seoul (MAPS-Seoul; May to June, 2015) and Korea-United States Air Quality Study (KORUS-AQ; May to June, 2016), field campaigns in Korea aimed to monitor and understand air quality (https://espo.nasa.gov/korus-aq/content/KORUS-AQ_Science_Overview_0). It also supports studies associated with the planned satellite mission for the Geostationary Environmental Monitoring Spectrometer (GEMS; Kim, 2012), designed to study atmospheric chemical composition and reaction mechanisms over East Asia (Kim *et al.*, 2017). Measurements from Pandora instruments in South Korea have been utilized for multi-year analyses and the validation of total O₃ measurements (Baek *et al.*, 2017; Kim *et al.*, 2017). Although the data quality of total O₃ from the Pandora spectrometers differs by instrument, the difference in total O₃ between Pandora and other instruments has been less than 2% in all comparison studies to date (Baek *et al.*, 2017; Kim *et al.*, 2017).

Because variations in total O₃ can primarily be attributed to changes in the stratosphere, the pattern of total O₃ density shows a weak dependence on regional or local emissions near the observation sites. In contrast, NO₂ column is affected primarily by vehicle emissions, industrial activities, and local short-range transport in the troposphere. Although some previous work analyzed the effect of the long-range transport of NO₂ (e.g., Donnelly *et al.*, 2015), the lifetime of NO₂ near the surface is on the order of hours to days

(Seinfeld and Pandis, 2012), indicating that a careful approach is required for analyses of the effects of regional-scale transport on variations in NO₂ concentrations.

Thus, the objective of this study is to investigate the effects of local air-mass transport from NO₂ sources on vertical column densities (VCD) of tropospheric NO₂ from Pandora observations. As a preliminary study for the KORUS-AQ campaign, we analyzed the regional characteristics of NO₂ measurements at six Pandora sites obtained during the MAPS-Seoul campaign while considering wind patterns and the locations of regional emission sources. Using these findings, we report the characteristics of NO₂ VCD during the MAPS-Seoul campaign from May 18 to June 14, 2015 in South Korea.

DATA AND ANALYSIS

Variations in tropospheric NO₂ VCD were analyzed at six Pandora sites. Also, the characteristics of NO₂ transport during the MAPS-Seoul campaign were investigated using the wind information from European Centre for Medium-Range Weather Forecasts (ECMWF) reanalysis data. To evaluate the characteristics of transport in the troposphere at the Pandora observation sites, we obtained tropospheric NO₂ VCD by subtracting Ozone Monitoring Instrument (OMI) stratospheric NO₂ VCD from Pandora total NO₂ VCD.

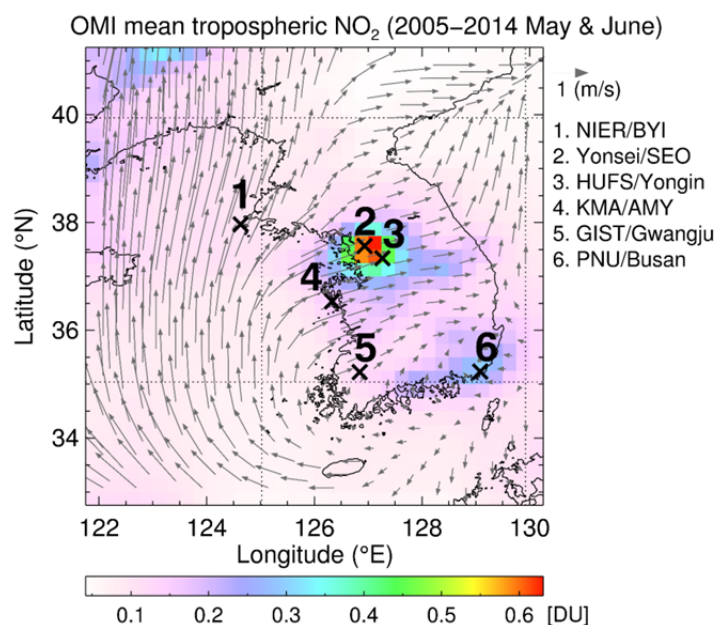
NO₂ from Pandora

The Pandora spectrometer system is configured with mounting systems for sun-tracker and sky-scanner controls, and a temperature stabilizing system for radiometric calibration (e.g., Herman *et al.*, 2009; Tzortziou *et al.*, 2012, 2013). The Pandora instruments in Korea are direct-sun (DS) spectrometer systems with a spectral range of 280–525 nm (spectral resolution: 0.42–0.52 nm for Full-Width at Half Maximum), and are used to measure the absorption spectra of trace gases (Baek *et al.*, 2017). The first two Pandora spectrometers in Korea were respectively installed at Yonsei University and Pusan National University in March 2012 to measure total column NO₂ and O₃. These instruments participated in the DRAGON-NE Asia campaign in South Korea at that time. Since the initial installations, six Pandora observation sites came into operation over the Korean Peninsula as part of the MAPS-Seoul campaign. Table 1 summarizes the locations and altitudes of the Pandora observation sites operated during the campaign. Fig. 1 shows their locations with a ten-year (2005–2014) mean tropospheric NO₂ VCD in Dobson Units (DU; 1 DU = 2.69×10^{16} molecules cm⁻²) from Level 3 OMI NO₂ product (OMNO2d) in May and June, and mean surface wind reanalysis data from ECMWF for the same period.

Total NO₂ VCD from Pandora was retrieved using the spectral fitting method described by Herman *et al.* (2009). For the analysis, we used Pandora level-3 data, which includes the normalized root-mean square error (normalized RMS), uncertainties in the NO₂ column, and the index of the filter wheel position. Threshold values for quality control that we used were 0.05 and 0.05 DU for normalized RMS and uncertainties in the NO₂ column, respectively.

Table 1. Location and altitude of each Pandora site during the MAPS-Seoul campaign.

Site	NIER/BYI	Yonsei/SEO	HUFS/Yongin	KMA/AMY	GIST/Gwangju	PNU/Busan
Longitude (°E)	124.631	126.934	127.265	126.330	126.843	129.083
Latitude (°N)	37.965	37.564	37.338	36.538	35.226	35.235
Altitude (m)	136	88	167	47	52	71

**Fig. 1.** Locations of the Pandora sites on the Korean Peninsula with a ten-year (2005–2014) mean tropospheric NO₂ VCD from OMI in May and June, and mean surface wind reanalysis data from ECMWF for the same period.

Pandora provides total NO₂ VCD every 80 seconds (e.g., Tzortziou *et al.*, 2012; Yun *et al.*, 2013). We converted the Pandora total NO₂ VCDs to hourly values by averaging over a ± 30 -min window every hour. In this procedure, the resultant hourly data which have less than three points in their windows ($\sim 5\%$ of total measurable points in an hour) were excluded. Total VCD includes both stratospheric and tropospheric NO₂. However, tropospheric NO₂ VCD usually dominates total NO₂ VCD variations near urban and industrial areas. To accurately estimate tropospheric NO₂ VCD from Pandora observations, stratospheric NO₂ information is required. For this information, we used the OMI standard product, which is explained in detail in the following subsection. Thus, tropospheric NO₂ VCD was estimated for the MAPS-Seoul campaign at each observation site, and the number of data points at each site is listed in Table 2. Because of problems with the tracker cable on the Pandora instrument at the Yonsei/SEO site beginning May 29, the number of valid data points at this site was less than half the number of data points at the other five Pandora observation sites.

The six Pandora sites were selected to include both urban and rural areas on the Korean Peninsula. Fig. 2 shows the topography (in color) of the regions around the observation sites. The Baengnyeongdo site operated by National Institute of Environmental Research (NIER) (NIER/BYI; Fig. 2(a)) and the Anmyeondo site operated by Korean Meteorological Agency (KMA) (KMA/AMY; Fig. 2(d)) are located in coastal areas far from industrial and urban regions. The

NIER/BYI site is on an island located in northwest South Korea and is the closest site to China. KMA/AMY is also located in the western coastal region of Korea. The NIER/BYI and KMA/AMY sites are relatively free from the urban pollution and therefore were used as background sites in this study. The Busan (operated by Pusan National University) (PNU/Busan; Fig. 2(f)) site and the Gwangju (operated by Gwangju Institute of Science and Technology; GIST) (GIST/Gwangju; Fig. 2(e)) site are located on the northern part of the urban areas in Busan and Gwangju, respectively. These two cities are respectively the 2nd and 6th most populous cities in South Korea. The Seoul (operated by Yonsei University) (Yonsei/SEO; Fig. 2(b)) site and the Yongin (operated by Hankuk University of Foreign Studies; HUFS) (HUFS/Yongin; Fig. 2(c)) site are located in the Seoul metropolitan area (SMA); however, these two sites have different characteristics. The Yonsei/SEO site is at the center of the Seoul urban area, while the HUFS/Yongin site is in a suburban area 40 km southeast and downwind of Seoul. Therefore, the HUFS/Yongin site is expected to be affected by transport from the urban area of Seoul.

Stratospheric NO₂ from OMI

The OMI instrument was designed to observe total column amounts of several trace gases including NO₂, and thus aid analyses of air quality and assessments of the climate effects of changes in chemical composition. OMI was launched in 2004 onboard the Aura satellite and

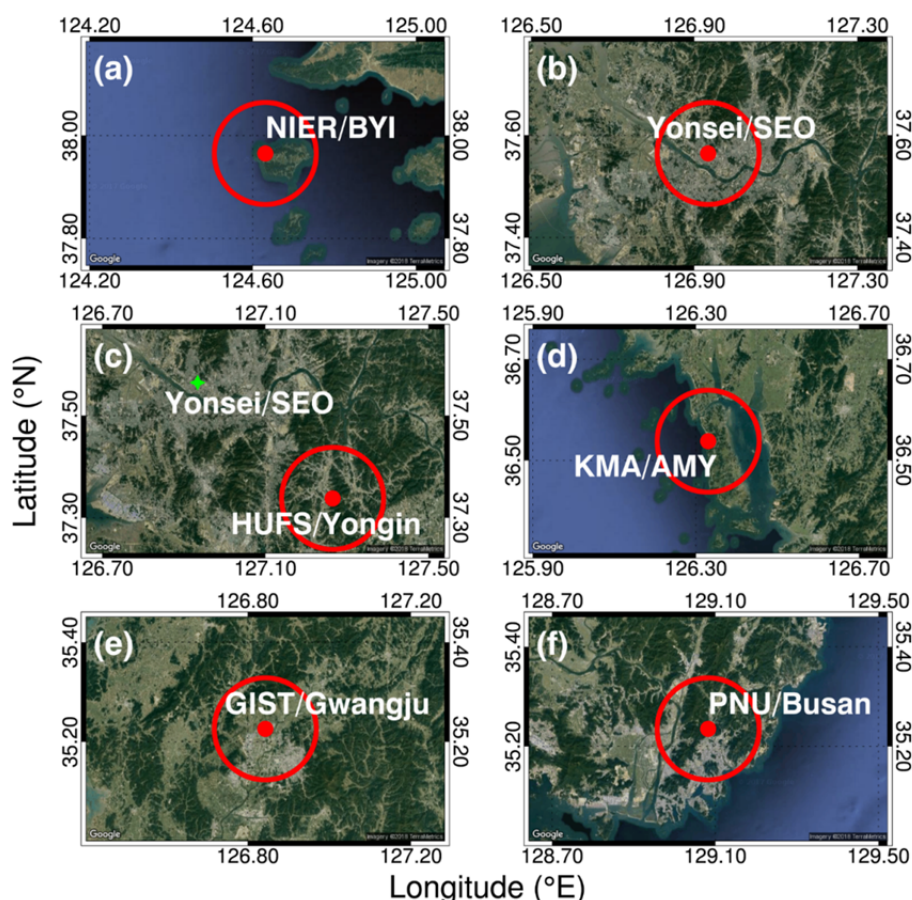


Fig. 2. Local characteristics of the Pandora sites at (a) NIER/BYI, (b) Yonsei/SEO, (c) HUFY/Yongin, (d) KMA/AMY, (e) GIST/Gwangju, and (f) PNU/Busan. The radius of each red circle is 0.125° , representing the resolution of the wind field we employed, and the center of it indicates the location of each Pandora (red dot). The location of Pandora at Yonsei/SEO is marked in green on (c) (Maps created using Google Earth Imagery).

measures backscattered solar light in the ultra violet (UV)-visible range (270–500 nm) using three different channels (two UV and one visible; e.g., Levelt *et al.*, 2006; Buchard *et al.*, 2008). The nominal spatial resolution is from $13 \times 24 \text{ km}^2$ (at nadir) to $28 \times 150 \text{ km}^2$ (at the edge of the swath). Because the Aura is a sun-synchronous satellite with a 98° inclination angle, daily values over the Korean Peninsula from OMI were obtained from data from one or two overpasses per day in the afternoon. The nadir pass was obtained close to 13:30 local time.

The NO_2 VCD from OMI is based on the level-2 standard product of NASA's version 3 OMI NO_2 (OMNO2) dataset. For the retrieval of NO_2 , spectral radiance data from 405 to 465 nm in the visible spectrum were used to estimate slant column amounts (Bucsela *et al.*, 2013). As part of improvements to the retrieval algorithm between versions 2 and 3, chemical transport model simulations with time-dependent emissions were adopted to account for variations in the vertical profiles for air mass factor calculations (Ialongo *et al.*, 2016; Krotkov *et al.*, 2017). The OMNO2 provides total, tropospheric, and stratospheric NO_2 VCDs. Thus, OMI stratospheric NO_2 data can be used to estimate the tropospheric NO_2 VCD from Pandora observations. Stratospheric NO_2 is affected by chemical reactions and

lightning activity (Noxon, 1979; Zhang *et al.*, 2000; Wenig *et al.*, 2004) and thus varies spatiotemporally. We sampled the stratospheric NO_2 VCD from OMI for each Pandora station, and thus the tropospheric NO_2 VCD from Pandora data was calculated as

$$\text{VCD}_{\text{PAN,Trop}} = \text{VCD}_{\text{PAN,Tot}} - \text{VCD}_{\text{OMI,Strat}} \quad (1)$$

where $\text{VCD}_{\text{PAN,Trop}}$, $\text{VCD}_{\text{PAN,Tot}}$, and $\text{VCD}_{\text{OMI,Strat}}$ are the tropospheric and total NO_2 VCD from Pandora, and the stratospheric NO_2 VCD from OMI, respectively.

For spatial co-location with Pandora, we selected the OMI pixels within 20 km from each Pandora site. While the Pandora total NO_2 VCD was calculated for each hour, OMI values occur only once daily, in the afternoon. This is one potential error source for using OMI to estimate tropospheric NO_2 VCD from the Pandora observations. In this study, we assumed the temporal and spatial distribution of stratospheric NO_2 was stable throughout the day and over the 20 km window. This approach is adapted from previous studies (e.g., Knepp *et al.*, 2015; Kollonige *et al.*, 2017) which estimated tropospheric NO_2 VCD by subtracting OMI stratospheric NO_2 VCD from Pandora total column NO_2 observations, assuming constant stratospheric NO_2

column on a daily basis under polluted conditions. In less polluted regions, such as NIER/BYI in this study, negative tropospheric NO₂ values can occur occasionally with this method. In addition, during the stratosphere-troposphere separation procedure for OMI NO₂ standard product, the stratospheric NO₂ VCD is smoothed interpreting features smaller than 300 km in scale in the initial estimate as tropospheric (Bucsela *et al.*, 2013). Thus, assuming negligible spatial variability in the 20 km window, which is much smaller, is reasonable. Fig. 3 shows the total NO₂ VCD observed from Pandora and sampled stratospheric NO₂ VCD from OMI for each site during the MAPS-Seoul campaign. Tropospheric NO₂ dominates total NO₂ VCD in the SMA (at Yonsei/SEO and HUFS/Yongin), and PNU/Busan, as can be inferred from Fig. 1. Despite showing lower levels of total NO₂ compared to those sites, the amounts and variability of NO₂ in the stratosphere at NIER/BYI, KMA/AMY, and GIST/Gwangju are relatively small in comparison to total, allowing stratospheric NO₂ VCD to be assumed constant on a daily basis. However, there were days for which no data from OMI were available within 20 km from a ground-based observation site. In this case, the averaged OMI stratospheric NO₂ VCD for that particular site over the course of the campaign period was used (red dots in Fig. 3(b)).

Wind Data

To analyze the transport characteristics of NO₂ at the observation sites, we used the wind speed and wind direction at the surface. Because surface wind varies significantly with surface conditions over small spatial scales, high-resolution wind information is required. For the wind analysis, U and

V (west–east and south–north, respectively) wind components at 10 m altitude from ECMWF reanalysis interim data (hereafter ERA-Interim) were used in this study (Dee *et al.*, 2011; <http://apps.ecmwf.int/datasets/>). To decrease local surface-condition effects on wind, the ECMWF ERA-Interim were used at the highest available horizontal resolution, $0.125^\circ \times 0.125^\circ$.

The U and V wind components from ERA-Interim were interpolated to the latitude and longitude of the respective Pandora sites. Then we converted them to the wind speed and direction at each site. The original reanalysis data have a temporal resolution of 6 hours. Thus, wind information was interpolated to a 1-hour resolution from the original 6-hour resolution after the spatial interpolation, for temporal co-location with the NO₂ data.

RESULTS AND DISCUSSION

Fig. 4 shows a time series of hourly-based tropospheric NO₂ VCD from the Pandora observations. During the MAPS-Seoul campaign period, tropospheric NO₂ VCDs at NIER/BYI and KMA/AMY were remarkably low, ranging from -0.07 to 0.45 DU and from 0.03 to 0.95 DU, respectively. However, large NO₂ VCDs were observed, up to 4.70 DU at Yonsei/SEO and 2.04 DU at PNU/Busan. While the difference between the maximum and minimum during the whole campaign period was less than 1 DU at NIER/BYI and KMA/AMY, a variation of 3.96 DU was observed in a single day on May 28 at Yonsei/SEO. Tropospheric NO₂ VCD was always below 0.45 DU at the NIER/BYI site because of the large distance from emission sources. At the NIER/BYI site, the tropospheric NO₂ VCD

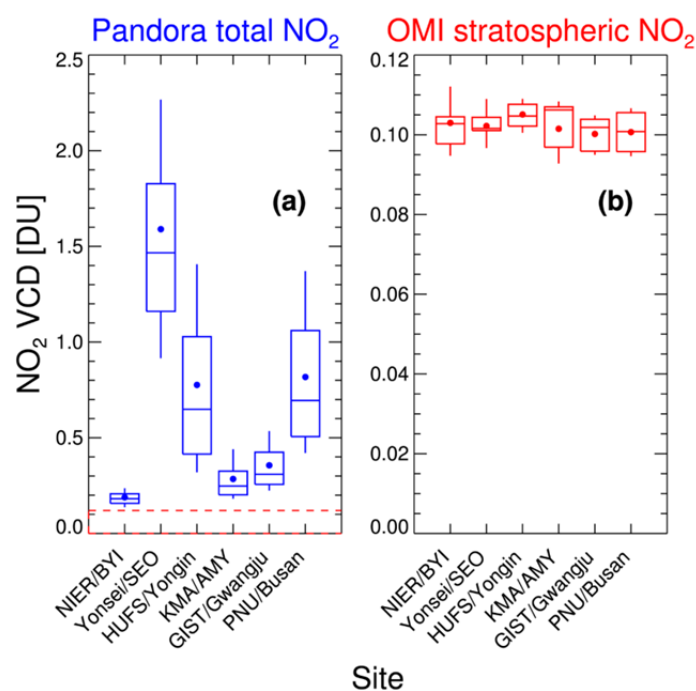


Fig. 3. (a) Total VCD of NO₂ observed from Pandora and (b) sampled stratospheric NO₂ from OMI at each site during the MAPS-Seoul campaign. Box-and-whisker plots show 10, 25, 50, 75, and 90 percentiles, and the dots indicate the means. The red box with broken lines in (a) represents the y-axis range of (b).

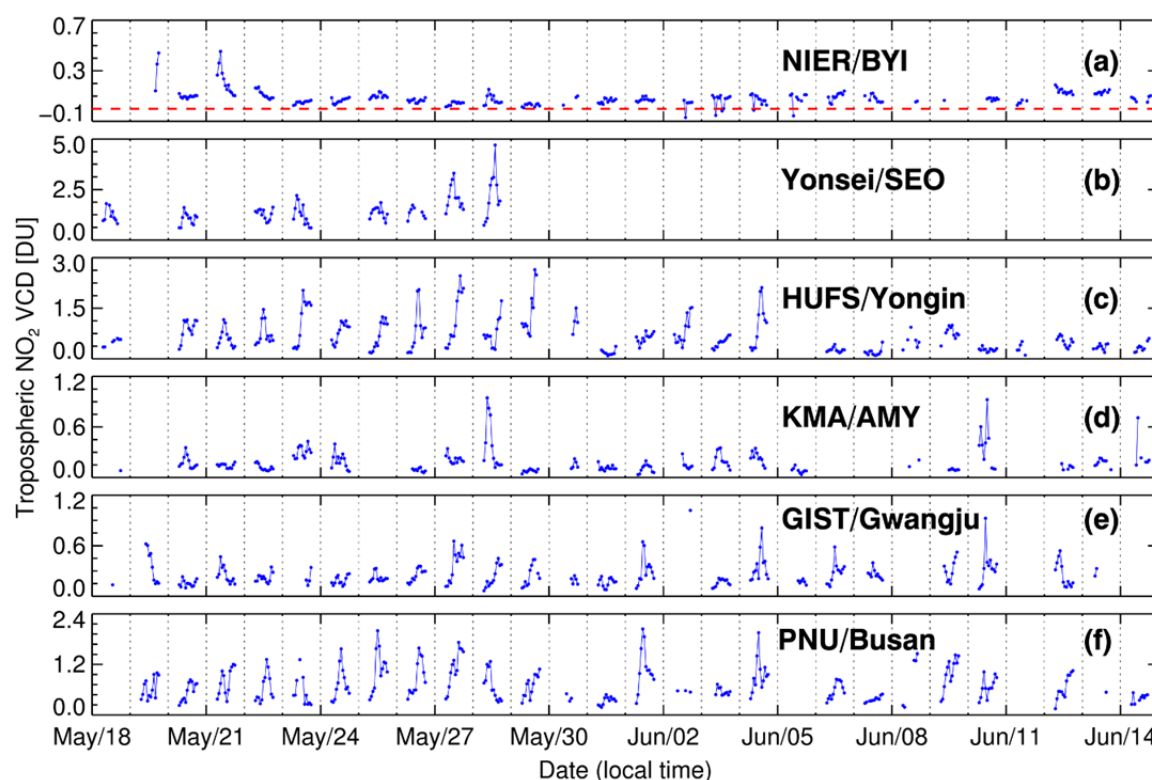


Fig. 4. Tropospheric NO₂ VCDs obtained from Pandora observations at the (a) NIER/BYI, (b) Yonsei/SEO, (c) HUFS/Yongin, (d) KMA/AMY, (e) GIST/Gwangju, and (f) PNU/Busan sites during the MAPS-Seoul campaign. The red broken line in (a) indicates 0 DU.

temporarily increased on May 19 and 21, but otherwise remained small and constant. Negative values were found at this site, which were generated by subtraction of OMI stratospheric NO₂ VCD larger than Pandora total NO₂ VCD. However, the number of them was less than 2% of the total data points. In a diurnal scale, variations in tropospheric NO₂ were clearly observed at the Yonsei/SEO, HUFS/Yongin, and PNU/Busan sites, which are the sites nearest to large urban areas. However, the diurnal cycle in tropospheric NO₂ VCD at GIST/Gwangju was not as strong. It was similar to what was observed at KMA/AMY and NIER/BYI, although the GIST/Gwangju site is located near an urban area (see also Fig. 9).

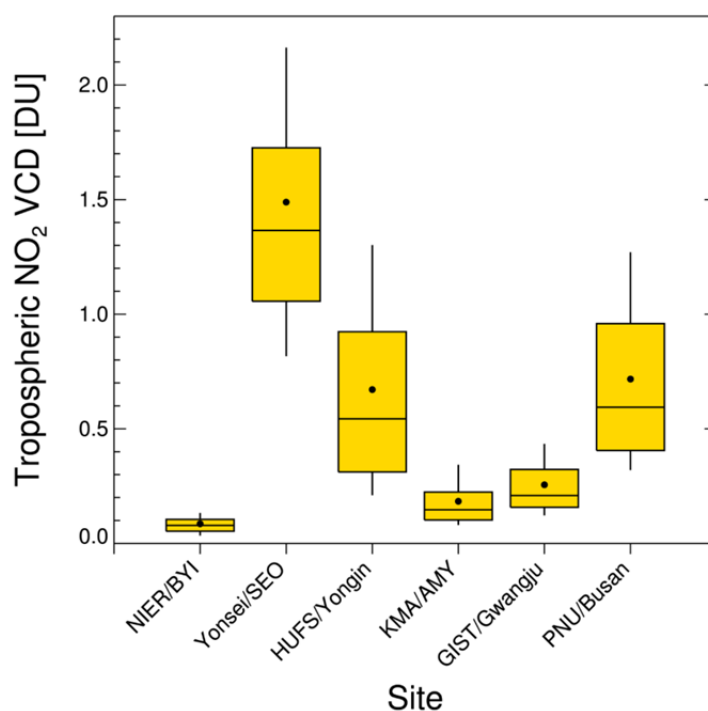
Table 2 and Fig. 5 present details of the hourly tropospheric NO₂ VCDs during the MAPS-Seoul campaign. The Yonsei/SEO site showed the maximum mean tropospheric NO₂ VCD (1.49 ± 0.68 DU) among the six sites during the campaign period. Even the minimum tropospheric NO₂ VCD at this site was 0.60 DU, which is larger than the maximum value of tropospheric NO₂ VCD at the NIER/BYI site (0.45 DU), representing the huge NO₂ emissions in Seoul. In addition, the HUFS/Yongin and PNU/Busan sites had similar tropospheric NO₂ VCD levels. The HUFS/Yongin site had the third largest average tropospheric NO₂ VCD (0.67 ± 0.49 DU), following PNU/Busan (0.72 ± 0.39 DU), indicating that huge local emissions in Seoul also lead to high NO₂ concentrations around the SMA. The NO₂ VCD in the troposphere at GIST/Gwangju (0.26 ± 0.14 DU) was comparable to that in KMA/AMY (0.18 ± 0.14 DU).

Although the GIST/Gwangju site is located in an urban area, levels of tropospheric NO₂ VCD resembled those at the suburban and rural sites, because the industrial region around Gwangju is small. As can be seen from the box-and-whisker plots in Fig. 5, all the sites are skewed in the positive direction. From the results so far, the statistics of tropospheric NO₂ were identified for each of the Pandora sites during the MAPS-Seoul campaign. However, even if the distribution of tropospheric NO₂ VCDs is similar among sites, major contributors to the amounts may differ depending on local emissions and transport patterns.

For better understanding of major contributors to tropospheric NO₂ VCD at each site, we need to examine the NO₂ VCD change in accordance with the wind pattern. Fig. 6 shows polar plots of tropospheric NO₂ VCD, along with wind speed and direction at the six Pandora sites. Because of the regional characteristics of wind and the short campaign period, it is likely that not all wind patterns in South Korea are included in the analysis (e.g., seasonal wind pattern). However, this analysis indicates how wind pattern affects the regional characteristics of tropospheric NO₂ during the MAPS-Seoul campaign. In most cases, the wind speed did not exceed 10 m s^{-1} at the observation sites, and westerly wind was dominant over easterly wind. This is consistent with the general wind pattern over the Korean peninsula in May and June (see Fig. 1). Despite the limited number of observed wind patterns, Fig. 6 clearly shows a change in tropospheric NO₂ VCD as the wind field changes. At all the Pandora observation sites, remarkably

Table 2. The statistics of tropospheric NO₂ VCD at each Pandora site during the MAPS-Seoul campaign. (Unit: DU).

Site	NIER/BYI	Yonsei/SEO	HUFS/Yongin	KMA/AMY	GIST/Gwangju	PNU/Busan
Average	0.09	1.49	0.67	0.18	0.26	0.72
Standard deviation	0.06	0.68	0.49	0.14	0.14	0.39
Maximum (Time)	0.45 (May 21 st , 09:00)	4.70 (May 28 th , 14:00)	2.65 (May 29 th , 15:00)	0.95 (May 28 th , 09:00)	1.02 (June 2 nd , 17:00)	2.04 (June 1 st , 11:00)
Minimum (Time)	−0.07 (June 2 nd , 14:00)	0.60 (May 20 th , 08:00)	0.09 (May 31 st , 13:00)	0.03 (June 5 st , 15:00)	0.07 (May 28 th , 07:00)	0.15 (June 12 th , 07:00)
Number of data points	251	88	272	211	238	256

**Fig. 5.** Tropospheric NO₂ VCD at each Pandora site. Box-and-whisker plots show 10, 25, 50, 75, and 90 percentiles, and the dots indicate the means.

high tropospheric NO₂ VCDs at each site were found for specific wind fields. However, these wind field characteristics differ among the observation sites.

At two urban sites, Yonsei/SEO (Fig. 6(b)) and PNU/Busan (Fig. 6(f)), high tropospheric NO₂ VCD values were found under conditions of southerly wind with low wind speed ($< 4 \text{ m s}^{-1}$). The GIST/Gwangju (Fig. 6(e)) site also showed high VCD values under these wind conditions, but the change in NO₂ VCD was smaller and may not be significant. This finding indicates that local NO₂ emissions have huge contribution to the enhancement of tropospheric NO₂ at Yonsei/SEO and PNU/Busan during the campaign period.

Specific wind fields at the NIER/BYI (Fig. 6(a)) and KMA/AMY (Fig. 6(d)) sites were also associated with high NO₂ VCD: westerly wind with speeds of $4\text{--}6 \text{ m s}^{-1}$ for NIER/BYI, and easterly wind with speeds of $2\text{--}4 \text{ m s}^{-1}$ for KMA/AMY. These two observation sites are in rural areas with weak local emissions. Therefore, high VCD values

can be attributed to transport. However, the NO₂ transport patterns differ between the two sites. As seen in Fig. 2, NIER/BYI borders the Yellow sea on the west, while the regions to the east of the KMA/AMY site are land surfaces. Therefore, high concentrations of NO₂ at the NIER/BYI site are thought to be due to trans-boundary transport (e.g., Lee *et al.*, 2014), while those at the KMA/AMY site are attributed to the transport of domestic (Korean) emissions near the observation sites. Large domestic sources of NO₂ around the KMA/AMY site include power plants and industrial activity. The KMA/AMY site is close to many power plants that provide power to the SMA, as well as several chemical plants. For this reason, easterly wind patterns change the characteristics of the KMA/AMY site from a classical rural site to those resembling an industrial site.

At the HUFS/Yongin site, high tropospheric NO₂ VCD values were found under northwesterly wind conditions with wind speeds of $2\text{--}6 \text{ m s}^{-1}$, as shown in Fig. 6(c). The

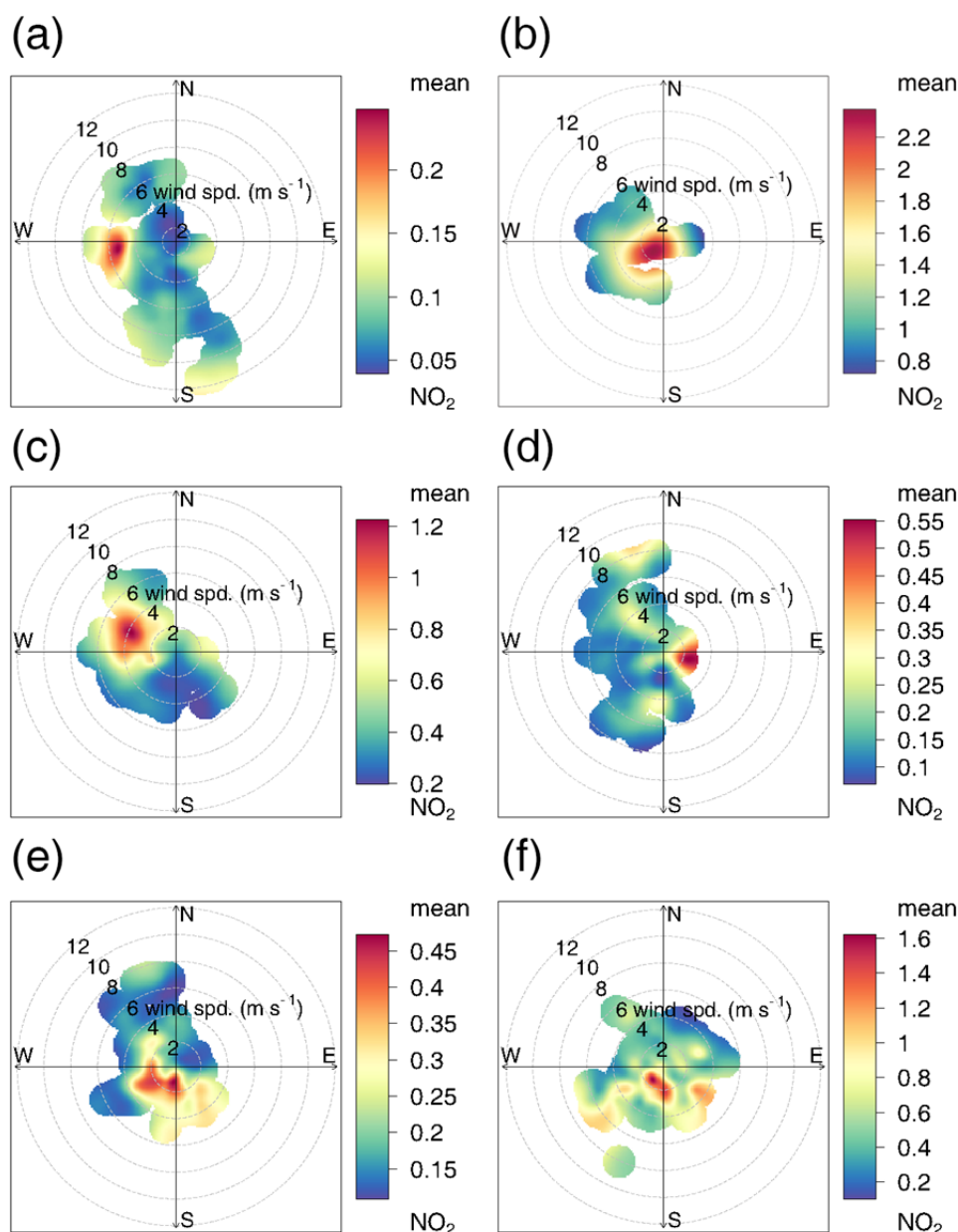


Fig. 6. Polar plots of tropospheric NO_2 VCD for the (a) NIER/BYI, (b) Yonsei/SEO, (c) HUFS/Yongin, (d) KMA/AMY, (e) GIST/Gwangju, and (f) PNU/Busan sites, along with wind conditions during the MAPS-Seoul campaign (Unit: DU).

HUFS/Yongin site is located on the southeast side of Seoul, making it downwind of Seoul during westerly wind conditions. Under these conditions, the air quality of the surrounding area is dominated by emissions from Seoul. Fig. 6(c) indicates that transport of pollutants from Seoul affected tropospheric NO_2 measurements at the HUFS/Yongin site during the MAPS-Seoul campaign. To further assess transport from Seoul to the HUFS/Yongin site, Fig. 7 shows a time series of tropospheric NO_2 VCD along with wind field data at the HUFS/Yongin site during the MAPS-Seoul campaign. Enhanced tropospheric NO_2 VCDs and high wind speed were highly connected under westerly wind conditions. Otherwise, low tropospheric NO_2 values were observed under conditions of weak wind speed or southwesterly winds. Considering the direction of Seoul

from the HUFS/Yongin site (Fig. 2(c)), those wind directions causing high tropospheric NO_2 VCD at HUFS/Yongin ($\sim 285^\circ$ – 345°) indicate that the HUFS/Yongin site was highly affected by NO_2 transport from Seoul.

Fig. 8 shows the correlation of tropospheric NO_2 VCDs between the HUFS/Yongin and Yonsei/SEO sites with consideration of the time difference. Because the distance between the Yonsei/SEO and HUFS/Yongin sites is about 40 km, the transport of NO_2 from Yonsei/SEO to HUFS/Yongin can be assessed using a time lag analysis between data from the two observation sites. For this assessment, tropospheric NO_2 VCD data were selected only for northwesterly wind conditions (a wind direction of 270° – 360°) at HUFS/Yongin, based on the relative location of the HUFS/Yongin site from the Yonsei/SEO site. A 3-hour

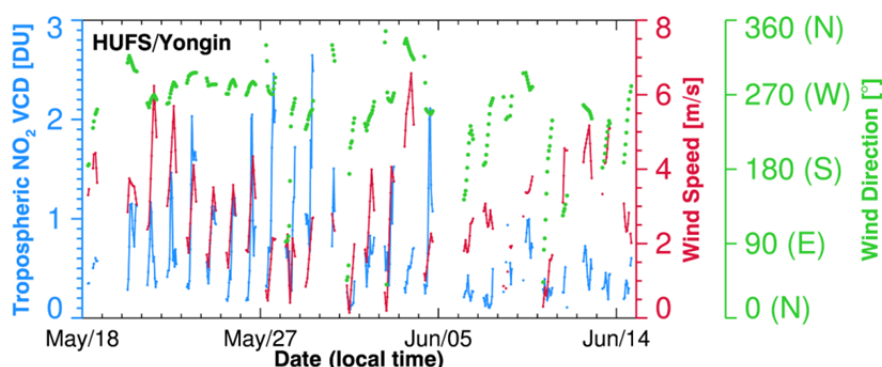


Fig. 7. Time series of tropospheric NO₂ VCD, wind speed, and wind direction at the HUFS/Yongin site.

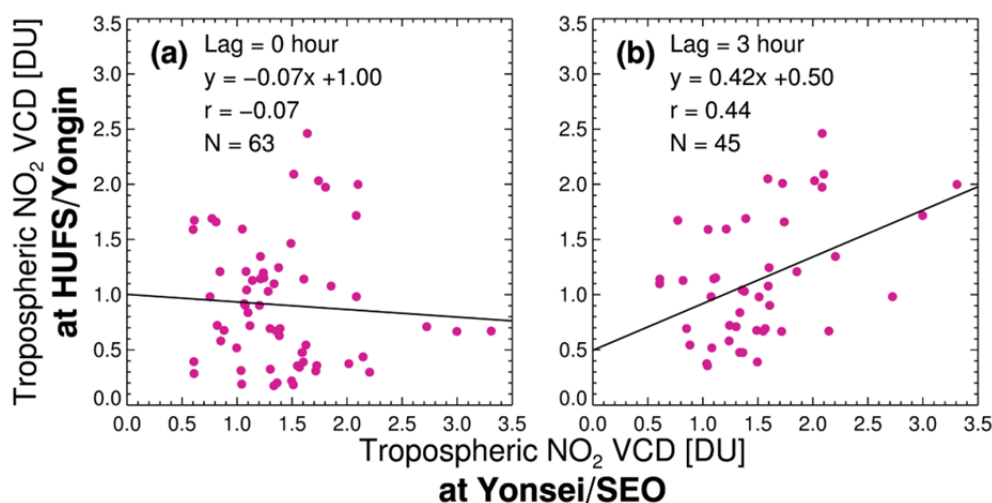


Fig. 8. Scatter plots of tropospheric NO₂ VCDs between the Yonsei/SEO and HUFS/Yongin sites (a) without consideration of time lag, and (b) with a time lag of 3 hours under northwesterly wind conditions at the HUFS/Yongin site.

time lag was used on the hourly HUFS/Yongin data for the lag correlation analysis shown in Fig. 8. In Fig. 8(a), no correlation was observed before adjusting for the time lag. Therefore, the tropospheric NO₂ VCDs observed at the same time at the two sites were not significantly related. After adjusting for the 3-hour time lag, however, a significant positive correlation was found with a correlation coefficient (r) of 0.44 (Fig. 8(b)). The time lag analysis indicated that tropospheric NO₂ in Seoul affects that at the HUFS/Yongin site within a few hours. As shown in Fig. 6(c), high tropospheric NO₂ VCDs at the HUFS/Yongin site were found when the wind was northwesterly at 2–6 m s⁻¹. Based on the distance between the two observation sites (~40 km) and the wind speed when tropospheric NO₂ concentrations were high at the HUFS/Yongin site, an air mass in Seoul would take 2–5 hours to flow to the HUFS/Yongin site.

Fig. 9 shows the average and standard deviation of hourly tropospheric NO₂ VCD during the MAPS-Seoul campaign. Because the Pandora instrument uses solar radiation, the temporal observation range is from 7:00 to 18:00, local time. In Fig. 9(a), a diurnal pattern of tropospheric NO₂ VCD is clearly seen for Yonsei/SEO. At Yonsei/SEO, NO₂ concentrations were high from 9:00 to 14:00. After high concentrations during the day, NO₂ VCD decreased in the

late afternoon. At the HUFS/Yongin site, however, the diurnal pattern of tropospheric NO₂ VCD was different from that in Yonsei/SEO. The tropospheric NO₂ VCD in the afternoon was higher than in the morning. Because of the lower transportation density around the HUFS/Yongin site, no effects on NO₂ VCD due to transportation during the morning rush hour were observed. The significant increase in NO₂ VCD during the afternoon may have been caused by NO₂ advection from Seoul, because the temporal change in tropospheric NO₂ VCD at HUFS/Yongin was highest between 12:00 and 13:00, 3 hours after VCD peaked in Yonsei/SEO. At PNU/Busan, NO₂ was high around noon, but was small compared with that observed at Yonsei/SEO, despite being a populous region. For the three regions in Fig. 9(a), the diurnal variations in tropospheric NO₂ VCD can be readily explained. However, an explanation of the diurnal variations in the remaining three regions (Fig. 9(b)) is more challenging because these three sites are strongly affected by wind field changes related to emission sources in the vicinity (KMA/AMY and GIST/Gwangju) and transboundary transport (NIER/BYI). At NIER/BYI, GIST/Gwangju, and KMA/AMY, we detected small diurnal variability in tropospheric NO₂ VCD during the MAPS-Seoul campaign.

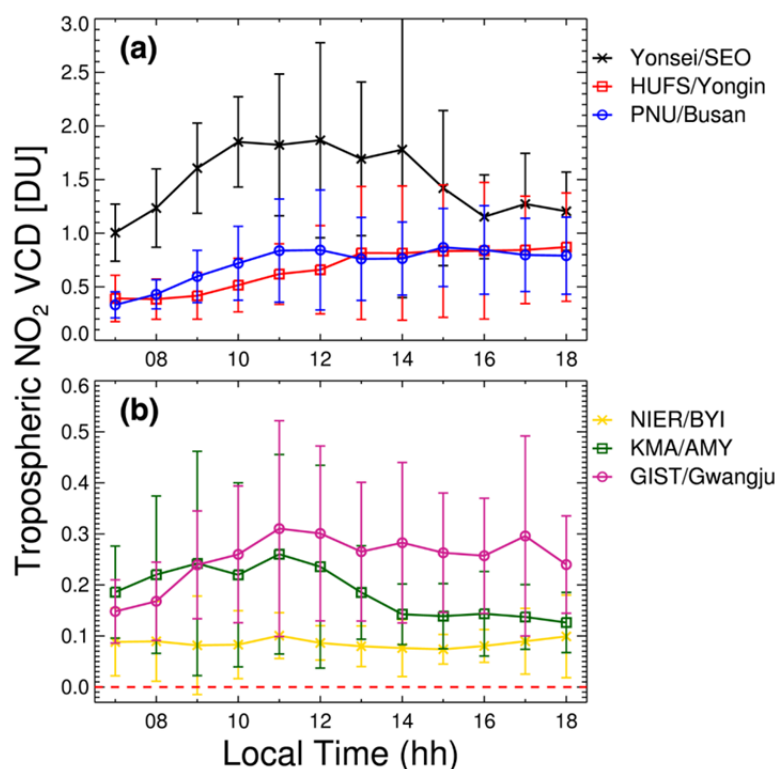


Fig. 9. Diurnal variations in tropospheric NO₂ at (a) Yonsei/SEO, HUFS/Yongin, and PNU/Busan, and (b) GIST/Gwangju, NIER/BYI and KMA/AMY, based on hourly averaged data. The error bars represent the standard deviations; the red broken line in (b) indicates 0 DU.

SUMMARY

NO₂ VCDs were observed at six Pandora observation sites on the Korean Peninsula during the MAPS-Seoul campaign from May to June 2015. To analyze NO₂ concentrations in the troposphere, we estimated the tropospheric NO₂ VCD at the six Pandora sites by subtracting OMI stratospheric NO₂ VCD from Pandora total NO₂ VCD. During the MAPS-Seoul campaign period, large differences in tropospheric NO₂ VCD were found between urban and rural sites. Two urban sites, Yonsei/SEO and PNU/Busan, had large maximum tropospheric NO₂ VCD values of 4.70 DU and 2.04 DU, respectively. However, tropospheric NO₂ VCD at the NIER/BYI site was always below 0.45 DU because of its large distance from emission sources. At the sites within the SMA (Yonsei/SEO and HUFS/Yongin), mean values of tropospheric NO₂ VCD were significantly larger than those at the other sites except for PNU/Busan. This indicates that regional emissions near Seoul significantly contribute to high NO₂ concentrations in the SMA. The tropospheric NO₂ VCD at GIST/Gwangju was comparable to that at KMA/AMY, even though the GIST/Gwangju site is located near an urban area.

To understand major contributors to tropospheric NO₂ VCD at each of the observation sites, the wind field (wind speed and direction) from reanalysis data at each site was analyzed in comparison with the change in NO₂ VCD. Using this method, high tropospheric NO₂ VCDs at each site were found to be related with specific wind speeds and

directions. At Yonsei/SEO and PNU/Busan, high tropospheric NO₂ VCD values were directly attributed to large local emissions. At the rural sites, the increase of NO₂ VCDs result primarily from trans-boundary transport (NIER/BYI) or transport from domestic emissions near the observation site (KMA/AMY). Because the location of HUFS/Yongin site is usually downwind of Seoul, high tropospheric NO₂ VCDs were found under conditions in which the wind blows directly from Seoul (i.e., strong northwesterly wind). In addition, tropospheric NO₂ VCD between the HUFS/Yongin and Yonsei/SEO sites was significantly correlated when a 3-hour time lag was included. This time lag is similar to the estimated transport time between the two sites, based on the distance between the two sites and the wind speed at which high tropospheric NO₂ VCD occurred. Therefore, it seems clear that the high tropospheric NO₂ VCD at HUFS/Yongin site can be directly attributed to emissions in Seoul.

Diurnal patterns in tropospheric NO₂ VCD are evident in Yonsei/SEO and HUFS/Yongin from daytime Pandora measurements, but no significant patterns were observed for NIER/BYI, KMA/AMY, and GIST/Gwangju. Although the Yonsei/SEO and HUFS/Yongin sites show diurnal variations in tropospheric NO₂ VCD, the nature of the variations differs between the two sites. At Yonsei/SEO, high NO₂ VCDs were found from 9:00 to 14:00. The HUFS/Yongin site did not show peaks in the morning, but high NO₂ VCDs were observed throughout the afternoon because of NO₂ transport from Seoul.

Tropospheric NO₂ VCD was analyzed at each site using Pandora observations. Throughout the campaign period, the SMA had higher NO₂ VCD than other areas in general. The lowest NO₂ value was observed at NIER/BYI. The relationship between NO₂ VCD and wind field was analyzed to investigate the effects of regional emissions and transport on the observation sites. The HUFY/Yongin site was significantly affected by the transport of emissions from Seoul. Although several notable results were obtained during this work, the analysis was limited to the period of the MAPS-Seoul campaign. Therefore, further analyses of variations in tropospheric NO₂ using data that span several years are required in the future.

ACKNOWLEDGMENTS

This subject is supported by Korea Ministry of Environment (MOE) as “Public Technology Program based on Environmental Policy (2017000160001)”. In addition, this research was also supported by the National Strategic Project-Fine Particle of the National Research Foundation of Korea (NRF) funded by the Ministry of Science and ICT (MSIT), the Ministry of Environment (ME), and the Ministry of Health and Welfare (MOHW) (Grant No. NRF-2017M3D8A1092021). We thank the site managers for installing and operating Pandora spectrometers in Korea during the MAPS-Seoul campaign period.

REFERENCES

- Allen, D., Pickering, K., Duncan, B. and Damon, M. (2010). Impact of lightning NO emissions on North American photochemistry as determined using the Global Modeling Initiative (GMI) model. *J. Geophys. Res.* 115: D22301.
- Baek, K., Kim, J.H., Herman, J.R., Haffner, D.P. and Kim, J. (2017). Validation of Brewer and Pandora measurements using OMI total ozone. *Atmos. Environ.* 160: 165–175.
- Barthe, C., Pinty, J.P. and Mari, C. (2007). Lightning-produced NO_x in an explicit electrical scheme tested in a Stratosphere-Troposphere Experiment: Radiation, Aerosols, and Ozone case study *J. Geophys. Res.* 112: D04302.
- Barton, P.K. and Atwater, J.W. (2002). Nitrous oxide emissions and the anthropogenic nitrogen in wastewater and solid waste. *J. Environ. Eng.* 128: 137–150.
- Bayram, H., Sapsford, R.J., Abdelaziz, M.M. and Khair, O.A. (2001). Effect of ozone and nitrogen dioxide on the release of proinflammatory mediators from bronchial epithelial cells of nonatopic nonasthmatic subjects and atopic asthmatic patients in vitro. *J. Allergy Clin. Immunol.* 107: 287–294.
- Boersma, K.F., Eskes, H.J. and Brinkema, E.J. (2004). Error analysis for tropospheric NO₂ retrieval from space. *J. Geophys. Res.* 109: D04311.
- Brasseur, G.P., Hauglustaine, D.A., Walters, S., Rasch, P. J., Muller, J.F., Granier, C. and Tie, X.X. (1998). MOZART, a global chemical transport model for ozone and related chemical tracers 1: Model description. *J. Geophys. Res.* 103: 28265–28289.
- Brewer, A.W., McElroy, C.T. and Kerr, J.B. (1973). Nitrogen dioxide concentrations in the atmosphere. *Nature* 246: 129–133.
- Buchard, V., Brogniez, C., Auriol, F., Bonnel, B., Lenoble, J., Tanskanen, A., Bojkov, B. and Veefkind, P. (2008). Comparison of OMI ozone and UV irradiance data with ground-based measurements at two French sites. *Atmos. Chem. Phys.* 8: 4517–4528.
- Bucsela, E.J., Krotkov, N.A., Celarier, E.A., Lamsal, L.N., Swartz, W.H., Bhartia, P.K., Boersma, K.F., Veefkind, J.P., Gleason, J.F. and Pickering, K.E. (2013). A new stratospheric and tropospheric NO₂ retrieval algorithm for nadir-viewing satellite instruments: Applications to OMI. *Atmos. Meas. Tech.* 6: 2607–2626.
- Castellanos, P., Boersma, K.F., Torres, O. and de Haan, J.F. (2015). OMI tropospheric NO₂ air mass factors over South America: effects of biomass burning aerosols. *Atmos. Meas. Tech.* 8: 3831–3849.
- Cede, A., Herman, J., Richter, A., Krotkov, N. and Burrows, J. (2006). Measurements of nitrogen dioxide total column amounts using a Brewer double spectrophotometer in direct sun mode. *J. Geophys. Res.* 111: D05304.
- Cede, A. (2011). *Manual for Pandora software suite. Version 1.3.*
- Chimot, J., Vlemmix, T., Veefkind, J.P., de Haan, J.F. and Levelt, P.F. (2016). Impact of aerosols on the OMI tropospheric NO₂ retrievals over industrialized regions: How accurate is the aerosol correction of cloud-free scenes via a simple cloud model? *Atmos. Meas. Tech.* 9: 359–382.
- Chitano, P., Hosselet, J., Mapp, C. and Fabbri, L. (1995). Effect of oxidant air pollutants on the respiratory system: Insights from experimental animal research. *Eur. Respir. J.* 8: 1357–1371.
- Choi, Y., Kim, J., Eldering, A., Osterman, G., Yung, Y.L., Gu, Y. and Liou, K.N. (2009). Lightning and anthropogenic NO_x sources over the United States and the western North Atlantic Ocean: Impact on OLR and radiative effects. *Geophys. Res. Lett.* 36: L17806.
- Choi, Y., Wang, Y., Zeng, T., Cunnold, D., Yang, E.S., Martin, R., Chance, K., Thouret, V. and Edgerton, E. (2008). Springtime transitions of NO₂, CO, and O₃ over North America: Model evaluation and analysis. *J. Geophys. Res.* 113: D20311.
- Crutzen, P.J. (1979). The role of NO and NO₂ in the chemistry of the troposphere and stratosphere. *Ann. Rev. Earth Planet. Sci.* 7: 443–472.
- Dee, D.P., Uppala, S.M., Simmons, A.J., Berrisford, P., Poli, P., Kobayashi, S., Andrae, U., Balmaseda, M.A., Balsamo, G., Bauer, P., Bechtold, P., Beljaars, A.C.M., van de Berg, L., Bidlot, J., Bormann, N., Delsol, C., Dragani, R., Fuentes, M., Geer, A.J., Haimberger, L., Healy, S.B., Hersbach, H., Hólm, E.V., Isaksen, I., Kållberg, P., Köhler, M., Matricardi, M., McNally, A. P., Monge-Sanz, B.M., Morcrette, J.J., Park, B.K., Peubey, C., de Rosnay, P., Tavaloto, C., Thépaut, J.N. and Vitart, F. (2011). The ERA-Interim reanalysis: Configuration and

- performance of the data assimilation system. *Q. J. R. Meteorolog. Soc.* 137: 553–597.
- Diemmoz, H., Siani, A.M., Redonas, A., Savastiouk, V., McElroy, C.T., Navarro-Comas, M. and Hase, F. (2014). Improved retrieval of nitrogen dioxide (NO_2) column densities by means of MKIV Brewer spectrophotometers. *Atmos. Meas. Tech.* 7: 4009–4022.
- Donnelly, A.A., Broderick, B.M. and Misstear, B.D. (2015). The effect of long-range air mass transport pathways on PM_{10} and NO_2 concentrations at urban and rural background sites in Ireland: Quantification using clustering techniques. *J. Environ. Sci. Health A* 50: 647–658.
- Galloway, J.N., Dentener, F.J., Capone, D.G., Boyer, E.W., Howarth, R.W., Seitzinger, S.P., Asner, G.P., Cleveland, C.C., Green, P.A., Holland, E.A., Karl, D. M., Michaels, A.F., Porter, J.H., Townsend, A.R. and Voeroesmary, C.J. (2004). Nitrogen cycles: Past, present, and future. *Biogeochemistry* 70: 153–226.
- Herman, J., Cede, A., Spinei, E., Mount, G., Tzortziou, M. and Abuhassan, N. (2009). NO_2 column amounts from ground-based Pandora and MFDOS spectrometers using the direct-sun DOAS technique: Intercomparisons and application to OMI validation. *J. Geophys. Res.* 114: D13307.
- Hudman, R.C., Jacob, D.J., Turquety, S., Leibensperger, E.M., Murray, L.T., Wu, S., Gilliland, A.B., Avery, M., Bertram, T.H., Brune, W., Cohen, R.C., Dibb, J.E., Flocke, F.M., Fried, A., Holloway, J., Neuman, J.A., Orville, R., Perring, A., Ren, X., Sachse, G.W., Singh, H.B., Swanson, A. and Wooldridge, P.J. (2007). Surface and lightning sources of nitrogen oxides over the United States: Magnitudes, chemical evolution, and outflow. *J. Geophys. Res.* 112: D12S05.
- Ialongo, I., Herman, J., Krotkov, N., Lamsal, L., Boersma, K.F., Hovila, J. and Tamminen, J. (2016). Comparison of OMI NO_2 observations and their seasonal and weekly cycles with ground-based measurements in Helsinki. *Atmos. Meas. Tech.* 9: 5203–5212.
- Intergovernmental Panel on Climate Change (IPCC) (2007). *Contribution of Working Group I to the Fourth Assessment Report of the Intergovernmental Panel on Climate Change, in Climate Change 2007: The Physical Science Basis*, Solomon, S. et al. (Eds.), 996 pp., Cambridge Univ. Press, Cambridge, U.K.
- Irie, H., Kanaya, Y., Akimoto, H., Tanimoto, H., Wang, Z., Gleason, J.F. and Bucsela, E.J. (2008). Validation of OMI tropospheric NO_2 column data using MAX-DOAS measurements deep inside the North China Plain in June 2006: Mount Tai Experiment 2006. *Atmos. Chem. Phys.* 8: 6577–6586.
- Kerr, J.B., Asbridge, I.A. and Evans, W.F.J. (1988). Intercomparison of total ozone measured by the Brewer and Dobson spectrophotometers at Toronto. *J. Geophys. Res.* 93: 11129–11140.
- Kerr, J.B. (1989). Ground-based measurements of nitrogen dioxide using the Brewer spectrophotometer. Ozone in the Atmosphere, Proceedings of the Quadrennial Ozone Symposium 1988 and Tropospheric Ozone Workshop held 4–13 August, 1988 in Göttingen, Federal Republic of Germany. Bojkov, R.D. and Fabian, P. (Eds.), A. Deepak Publishing, Hampton, VA, 1989, p. 340.
- Kim, J. (2012). GEMS (Geostationary Environmental Monitoring Spectrometer) onboard the GeoKOMPSAT to monitor air quality in high temporal and spatial resolution over Asia-Pacific Region. EGU General Assembly 2012, held 22–27 April, 2012 in Vienna, Austria, p.4051.
- Kim, J., Kim, J., Cho, H.K., Herman, J., Park, S.S., Lim, H.K., Kim, J.H., Miyagawa, K. and Lee, Y.G. (2017). Intercomparison of total column ozone data from the Pandora Spectrophotometer with Dobson, Brewer and OMI measurements over Seoul, Korea. *Atmos. Meas. Tech.* 10: 3661–3676.
- Knepp, T., Pippin, M., Crawford, J., Chen, G., Szykman, J., Long, R., Cowen, L., Cede, A., Abuhassan, N., Herman, J., Delgado, R., Compton, J., Berkoff, T., Fishman, J., Martins, D., Stauffer, R., Thompson, A., Weinheimer, A., Knapp, D., Montzka, D., Lenschow, D. and Neil, D. (2015). Estimating surface NO_2 and SO_2 mixing ratios from fast-response total column observations and potential application to geostationary missions, *J. Atmos. Chem.* 72: 261–286.
- Kollonige, D.E., Thompson, A.M., Josipovic, M., Tzortziou, M., Beukes, J.P., Burger, R., Martins, D.K., van Zyl, P.G., Vakkari, V. and Laakso, L. (2017). OMI satellite and ground-based Pandora observations and their application to surface NO_2 estimations at terrestrial and marine sites. *J. Geophys. Res.* 123: 1441–1459.
- Krotkov, N.A., Lamsal, L.N., Celarier, E.A., Swartz, W.H., Marchenko, S.V., Bucsela, E.J., Chan, K.L., Wenig, M. and Zara, M. (2017). The version 3 OMI NO_2 standard product. *Atmos. Meas. Tech.* 10: 3133–3149.
- Lee, D.S., Koehler, J., Grobler, E., Rohrer, F., Sausen, R., Gallardo-Klenner, L., Olivier, J.G.J., Dentener, F.J. and Bouwman, A.F. (1997). Estimations of global NO_x emissions and their uncertainties. *Atmos. Environ.* 31: 1735–1749.
- Lee, H., Irie, H., Kim, Y.J., Noh, Y., Lee, C., Kim, Y. and Chun, K.J. (2009a). Retrieval of aerosol extinction in the lower troposphere based on UV MAX-DOAS measurements. *Aerosol Sci. Technol.* 43: 502–509.
- Lee, H., Kim, Y.J., Jung, J., Lee, C., Heue, K.P., Platt, U., Hu, M. and Zhu, T. (2009b). Spatial and temporal variations in NO_2 distributions over Beijing, China measured by imaging differential optical absorption spectroscopy. *J. Environ. Manage.* 90: 1814–1823.
- Lee, H.J., Kim, S.W., Brioude, J., Cooper, O.R., Frost, G.J., Kim, C.H., Park, R.J., Trainer, M. and Woo, J.H. (2014). Transport of NO_x in East Asia identified by satellite and in situ measurements and Lagrangian particle dispersion model simulations. *J. Geophys. Res.* 119: 2574–2596.
- Levelt, P.F., Van den Oord, G.H., Dobber, M.R., Malkki, A., Visser, H., De Vries, J., Stammes, P., Lundell, J.O. and Saari, H. (2006). The ozone monitoring instrument, *IEEE Trans. Geosci. Remote Sens.* 44: 1093–1101.
- Liley, J.B., Johnston, P.V., McKenzie, R.L., Thomas, A.J.

- and Boyd, I.S. (2000). Stratospheric NO₂ variations from a long time series at Lauder, New Zealand. *J. Geophys. Res.* 105: 11633–11640.
- Noxon, J.F. (1979). Stratospheric NO₂ global behavior. *J. Geophys. Res.* 84: 5067–5076.
- Seinfeld, J.H. (1988). Ozone air quality models. *JAPCA* 38: 616–645.
- Seinfeld, J.H. and Pandis, S.N. (2012). *Atmospheric chemistry and physics: From air pollution to climate change*, John Wiley & Sons, 225 pp.
- Sinreich, R., Friess, U., Wagner, T. and Platt, U. (2005). Multi axis differential optical absorption spectroscopy (MAX-DOAS) of gas and aerosol distributions. *Faraday Discuss.* 130: 153–164.
- Solomon, S., Portmann, R.W., Sanders, R.W., Daniel, J.S., Madsen, W., Bartram, B. and Dutton, E. G. (1999). On the role of nitrogen dioxide in the absorption of solar radiation. *J. Geophys. Res.* 104: 12047–12058.
- Tzortziou, M., Herman, J. R., Cede, A. and Abuhassan, N. (2012). High precision, absolute total column ozone measurements from the Pandora spectrometer system: Comparisons with data from a Brewer double monochromator and Aura OMI. *J. Geophys. Res.* 117: D16303.
- Tzortziou, M., Herman, J.R., Cede, A., Loughner, C.P., Abuhassan, N. and Naik, S. (2013). Spatial and temporal variability of ozone and nitrogen dioxide over a major urban estuarine ecosystem. *J. Atmos. Chem.* 72: 287–309.
- Van Roozendael, M., de Maziere, M., Hermans, C., Simon, P.C., Pommereau, J.P., Goutail, F., Tie, X.X., Brasseur, G. and Granier, C. (1997). Ground-based observations of stratospheric NO₂ at high and midlatitudes in Europe after the Mount Pinatubo eruption. *J. Geophys. Res.* 102: 19171–19176.
- von Klot, S., Peters, A., Aalto, P., Bellander, T., Berglind, N., D'Ippoliti, D., Elosua, R., Hörmann, A., Kulmala, M. and Lanki, T. (2005). Ambient air pollution is associated with increased risk of hospital cardiac readmissions of myocardial infarction survivors in five European cities. *Circulation* 112: 3073–3079.
- Wenig, M., Kuhl, S., Beirle, S., Bucsela, E., Jahne, B., Platt, U., Gleason, J. and Wagner, T. (2004). Retrieval and analysis of stratospheric NO₂ from the Global Ozone Monitoring Experiment. *J. Geophys. Res.* 109: D04315.
- Yun, S., Lee, H., Kim, J., Jeong, U., Park, S.S. and Herman, J. (2013). Inter-comparison of NO₂ column densities measured by Pandora and OMI over Seoul, Korea. *Korean J. Remote Sens.* 29: 663–670.
- Zhang, R., Sanger, N.T., Orville, R.E., Tie, X., Randel, W. and Williams, E.R. (2000). Enhanced NO_x by lightning in the upper troposphere and lower stratosphere inferred from the UARS Global NO₂ measurements. *Geophys. Res. Lett.* 27: 685–688.
- Zhang, X., Helsdon, J.H. and Farley, R.D. (2003). Numerical modeling of lightning-produced NO_x using an explicit lightning scheme: 2. Three dimensional simulation and expanded chemistry. *J. Geophys. Res.* 108: 4580.

Received for review, September 30, 2017

Revised, January 19, 2018

Accepted, January 20, 2018